HTML ABSTRACT + LINKS

Effect of nanoscale surface morphology on the phase stability of 3C-AlN films on Si(111)

V. Lebedev,[a] V. Cimalla, U. Kaiser, Ch. Foerster, J. Pezoldt, J. Biskupek, and O. Ambacher
Center of Micro- und Nanotechnology, Technical University Ilmenau, Postfach 100565, D98684 Ilmenau, Germany

(Received 16 December 2004; accepted 29 March 2005; published online 24 May 2005)

In this work, we report on the stabilization of 3C-AlN polytype by molecular-beam epitaxy (MBE) on 3C-SiC/Si(111) pseudosubstrates. The main purpose of the present studies is to analyze the mechanisms forcing the epitaxy of the 3C-AlN at typical MBE conditions. The forces driving the cubic polytype formation have been considered including supersaturation, macroscopic stress, interfacial energy, and interface morphology. We conclude that the growth of 3C-AlN phase can be stabilized on the "rough" 3C-SiC(111) surface by the polytype replication due to the lateral character of the nucleation and the reduction in the total energy of the film provided by periodical undulations of the template surface. © *2005 American Institute of Physics*.
[DOI: 10.1063/1.1915535]

I. INTRODUCTION

Wide-band-gap III-nitrides have attracted attention since the commercialization of bright blue light-emitting diodes and laser diodes.[1] Among them, AlN is being intensely investigated for possible electronic and optoelectronic applications since the early 1990s. The wide band gap afforded by aluminum nitride coupled with heterojunction capability pave the way for UV optoelectronics[2] and high-power electronic applications. Piezoelectric properties of AlN are feasible for application in surface acoustic wave (SAW) devices. Having a reasonable thermal match to Si, AlN also is an attractive material to accomplish the integration of III-nitride optoelectronic devices with Si-integrated circuits.

Three common crystal structures are shared by the tetrahedrally coordinated binary nitrides: rocksalt ($Fm\underline{3}m$), wurtzite ($2H, P6_3mc$), and zinc blende (ZB) ($3C, F\underline{4}3m$). The two latter structures differ only in the relative handedness of the fourth interatomic bond along the (111) chain (ABAB… for 2H and ABCABC… for 3C, see Refs. 3 and 4). These rather subtle structural differences and relatively small differences in the internal energies ($\Delta E_{\mathrm{W-ZB}}$) for the majority of binary compounds are manifested by the well-known 2H-3C polytypism. Despite the structural similarities, the optoelectronic properties of the wurtzite and cubic phases can be very different. In the case of III-nitrides, the 3C phase offers many potential advantages such as a high symmetry, lack of spontaneous polarization effects, and it is more suitable to p doping.[5] In particular, 2H-AlN ($a=3.11$ Å, $c=4.98$ Å) is a direct band-gap compound with $E_g \approx 6.2$ eV, while the band structure of the 3C-AlN ($a_0=4.38$ Å) is still under intensive debates due to the lack of high-quality 3C film. Among the theoretical predictions, Miao and Lambrecht[6] and Rubio *et al.*[7] reported on the band-structure calculations for 3C-AlN and the estimated value of the minimum indirect gap ($\Gamma_{15}^{v}-X_1^{c}$) to be of 4.9 ± 0.2 eV and minimum direct band gap at Γ point of ~6.24 eV. Recently, we showed that for the mixed-phase 3C-AlN epilayers (15% of 2H inclusions) the positions of the critical points in the band structure have a clear shift corresponding to the first direct transition at the Γ point at 5.74 eV.[8] However, an indirect transition at lower energies as proposed for the X point[9] could not be identified.

Depending on the epitaxial conditions, AlN thin films can be deposited in either forms.[10] However, the largest among the III-nitrides 2H-3C energy difference ($\Delta E_{\mathrm{W-ZB}} \sim -18.41$ meV/at. (Ref. 4) and ~43 meV/at. (Ref. 11)) forces the 2H phase of AlN to dominate at the usual growth conditions. Additionally, the lower symmetry of the 2H structure allows a distortion along the c axis. The $c/a_{\mathrm{2H\text{-}AlN}} \approx 1.601$ ratio and the internal cell parameter $u \approx 0.381$ (which determines the position of the anion relative to the cation sublattice) deviate significantly from their ideal values $c/a = (8/3)^{1/2} \approx 1.633$ and $u=3/8$. The close empirical correlation between c/a and the 2H vs 3C stability ($\Delta E_{\mathrm{W-ZB}}$) has been demonstrated by Lawaetz.[3] It was established that for the majority of binary III-V and II-VI compounds, $c/a < 1.633$ favors the 2H phase over the 3C one when growing epitaxially.

High-quality 2H-AlN films have been grown by the authors on various surfaces having different geometries and lattice parameters including threefold [Si(111) and 3C-SiC(111)] and fourfold [Si(001)] symmetry surfaces.[10] In all cases, the thermodynamical stability of the 2H phase overcomes the topological compatibility to the substrate.

There are a few reports on the epitaxy of c-AlN films stabilized by the lattice replication of the cubic substrate [for instance, Si(001)].[12–16] Up to date, the crystal quality of the 3C-AlN epilayers is still a challenge. The rocksalt phase has also been stabilized in the nonisostructural multilayer systems [such as AlN/VN (Ref. 17) and AlN/TiN (Ref. 18)]

[a]Electronic mail: vadim.lebedev@tu-ilmenau.de

 © 2005 American Institute of Physics

Downloaded 13 Jun 2005 to 141.24.27.92. Redistribution subject to AIP license or copyright, see http://jap.aip.org/jap/copyright.jsp

due to the "template effect" of the VN or TiN layer. In such systems, the cubic phase can exist only over a certain range of thickness (2–6 nm).

In this work we report on the stabilization of the 3C-AlN films by the growth on 3C-SiC/Si(111) pseudosubstrates. The main purpose of this work is to determine the mechanisms forcing the epitaxy of the metastable 3C polytype at the growth conditions typical for the plasma-induced molecular-beam epitaxy (PIMBE). The main forces driving the cubic polytype formation will be analyzed such as supersaturation, macroscopic stress, interfacial energy, and interface morphology. Conventional and high-resolution transmission electron microscopy (TEM) and x-ray diffraction (XRD) have been used to study the crystalline structure of the epilayers.

II. EXPERIMENT

Nominally undoped AlN epilayers were grown on 3C-SiC/Si(111) templates at 860 °C by PIMBE equipped with conventional effusion cells for group-III elements and a radio-frequency N_2 plasma source (Oxford Applied Research MDP21). The templates have been prepared by carbonization of Si substrates using (i) an ultrahigh-vacuum chemical-vapor deposition (UHVCVD), and (ii) a rapid thermal CVD (RTCVD). The *p*-type, *B*-doped, 2-in. Si(111)±0.5° wafers have been cleaned prior to the carbonization by a standard Radio Corporation of America (RCA) procedure. For the UHVCVD carbonization a mixture of ethene and hydrogen has been used at temperatures below 900 °C. The RTCVD carbonization has been performed using a mixture of 15% of ethene in H_2 during 60 s with a final temperature of 1280 °C. The detailed report on the carbonization experiments can be found elsewhere.[19]

On both types of the templates, the two-step growth of AlN has been carried out: nucleation and growth of a 30–40-nm-thick midtemperature AlN buffer layer ($T_{sub}\sim 630$ °C) followed by the temperature ramp (50 K/min). The grown layers have a final thickness of ~200–300 nm. The lattice constants and the resulting strain were determined by XRD reciprocal space mapping technique. The phonon spectra in the infrared range were taken between 400 and 4000 cm^{-1} using a SE 900 Fourier-transform-infrared-based spectroscopic ellipsometry (FTIR-SE).

III. EXPERIMENTAL RESULTS

Both UHVCVD and RTCVD carbonization processes result in well-oriented single-crystalline 3C-SiC layers with an average thickness of ~3 nm. The epitaxial relationship is $[111]_{3C\text{-}SiC}//[111]_{Si}$ and $[1\underline{1}0]_{3C\text{-}SiC}//[1\underline{1}0]_{Si}$. For the RTCVD carbonization a "quasi-two-dimensional" nucleation was used, which results in atomically flat SiC surfaces with a stepped morphology.[19] In the case of the UHVCVD carbonization, the Stranski–Krastanov–like nucleation bears a rougher morphology including surface undulations with a typical width and amplitude of 15–25 nm and 1–2 nm, respectively, as well as sporadic pits until the silicon substrate with an area density of 2% [see Fig. 5(b)]. A detailed discussion on the growth mechanism can be found in Ref. 19.

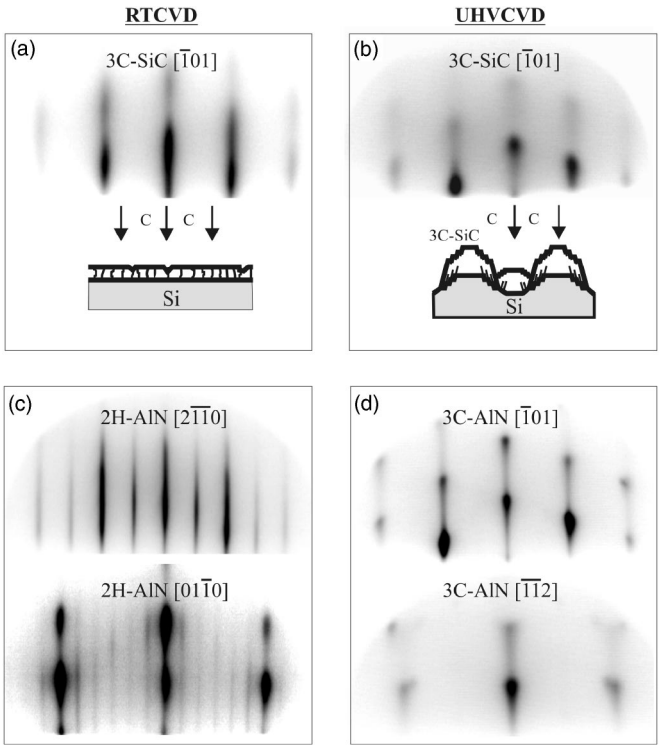

FIG. 1. The RHEED patterns of the 3-nm-thick 3C-SiC layers carbonized (a) by the RTCVD and (b) by the UHVCVD; (inserts: graphical presentation of the SiC carbonization model). RHEED pattern of (c) a 200-nm-thick 2H-AlN layer on a 3C-SiC(111) RTCVD template (2×6) and (d) a 200-nm-thick 3C-AlN layer on a 3C-SiC(111) UHVCVD template (1×1).

2H-AlN(0001) epilayers have been grown on RTCVD-prepared 3C-SiC(111) thin layers. Prior to the epitaxy, reflection high-energy electron diffraction (RHEED) revealed well-developed 3C-SiC $\bar{1}01$ "streaks" indicating flat surface conditions [Fig. 1(a)]. The nucleation and subsequent 2H-AlN growth have been maintained in the two-dimensional (2D) mode monitored by RHEED [Fig. 1(c)]. The atomic force microscopy (AFM) images demonstrated flat terraces on the 2H-AlN surface (width of ~150–200 nm and height of ~2 nm) due to ~0.5° off-axis angle of the Si(111) surface [Fig. 2(a)].

In contrast to the RTCVD case, UHVCVD-prepared 3C-SiC(111) films has a three-dimensional (3D) surface morphology [Fig. 1(b)]. The 3C-AlN(111) growth has been performed at low supersaturations, just on the boundary between 3D and 2D epitaxies [RHEED pattern in Fig. 1(d)] resulting in the rough surface of the grown films [Fig. 2(b)]. The use of higher supersaturations for Al resulting in smoother surface conditions leads to the immediate 2H-AlN nuclei formation followed by the development of 2H islands. Figure 3(b) demonstrates such 2H inclusion nucleated on the 3C surface during short-time (~60 s) Al-rich epitaxy and then overgrown by the 3C phase when the Al flux has been reduced to maintain stochiometric growth conditions.

The polytype of the AlN layers was confirmed by XRD experiments. $\omega/2\theta$ scans along the symmetric (111) and the asymmetric (224) for the 3C-AlN, and along the symmetric (002) and the asymmetric (20.5) for 2H-AlN have been performed. The symmetric reflexes of both polytypes are shown

Downloaded 13 Jun 2005 to 141.24.27.92. Redistribution subject to AIP license or copyright, see http://jap.aip.org/jap/copyright.jsp

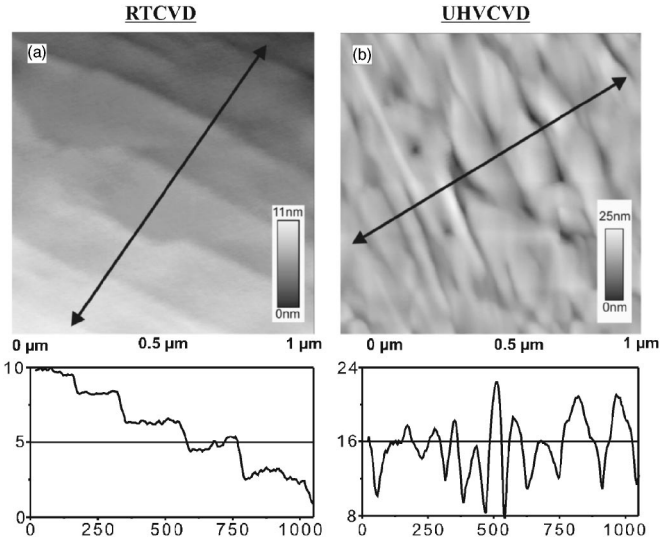

FIG. 2. AFM images of AlN films nucleated on the 3-nm-thick 3C-SiC layer carbonized (a) by the RTCVD (2H-AlN) and (b) by the CVD (3C-AlN).

in Fig. 3(a). It clearly demonstrates that pure 2H- and predominant 3C-AlN have been grown on flat RTCVD and "rough" CVD-carbonized Si(111) surfaces, respectively. In the case of the 3C-AlN a content of ~15% of 2H-AlN could be detected being in accordance with TEM and Raman spectroscopy observations.

Figure 3(c) shows a bright-field (bf) TEM micrograph of the 3C-AlN epilayer. The selected area electron-diffraction (SAED) pattern clearly demonstrates the cubic phase and the lattices relationship between the layer and the substrate. As a

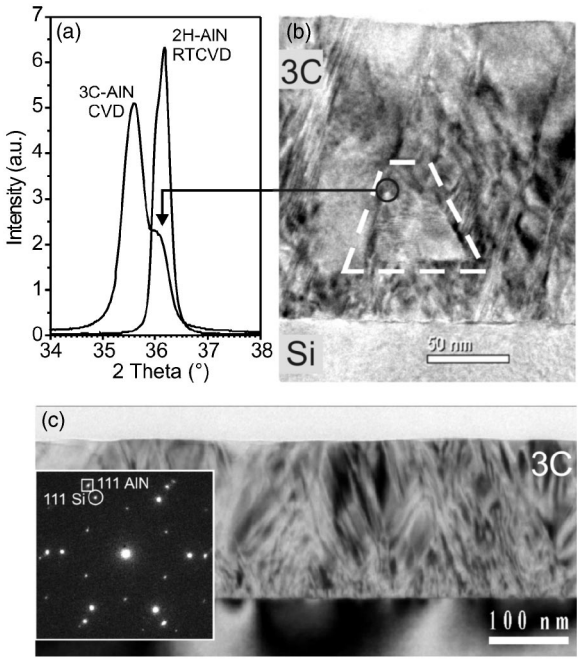

FIG. 3. (a) $\omega/2\theta$ scans for 2H-AlN layers grown on RTCVD carbonized and predominant 3C-AlN grown on UHVCVD-carbonized Si substrates. (b) 110 bright-field (bf) TEM image of the 3C-AlN layer showing 2H domain grown in higher supersaturation conditions. (c) 110 bf-TEM image of the 3C-AlN layer grown on the UHVCVD 3C-SiC(111) "rough" template showing stacking faults and twins in inclined {111} planes [insert: corresponding selected area electron diffraction (SAED) pattern].

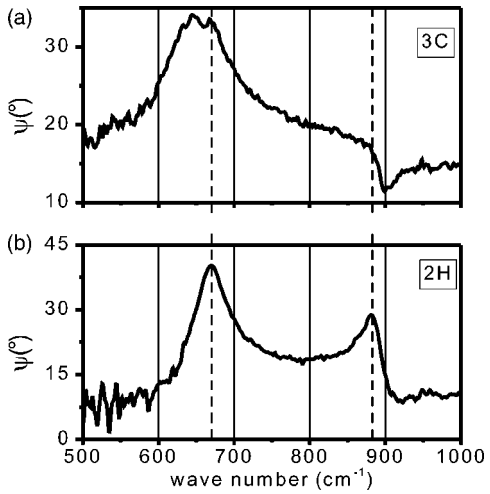

FIG. 4. FTIR-SE ψ spectra of (a) predominant 3C-(~12% of hexagonal inclusions) and (b) pure 2H-AlN films.

result of the low stacking fault (SF) energy in 3C-AlN, a high density of SFs/twins are created in {111} planes. The SFs, bounded by Shockley partial dislocations, are mostly spread throughout the layer creating a step on its surface.

Finally, the FTIR-SE and Raman measurements provided us with the zone-center optical-phonon frequencies in the 3C-AlN. Figure 4 shows the FTIR-SE ψ spectra for pure 2H-AlN and predominant 3C-AlN films. For the latter, the phonon frequencies were located at 631, 646.0, and 667.0 cm^{-1}. The peaks at $\omega^c_{TO}=646(631)$ cm^{-1} (corresponding to a value of $\sigma_{xx}=-9$ GPa) and shoulder with an onset of $\omega^c_{LO}=911$ cm^{-1} can be attributed to the 3C-AlN phase.[13,20] The analysis also revealed the residual 2H-phase contribution in the phonon spectra of 3C layers. The peak at 667 $cm^{-1}(E_1\text{-}\omega^h_{TO})$ and the shoulder with an onset of ~880 $cm^{-1}(A_1\text{-}\omega^h_{LO})$ have been detected, indicating the presence of the tensile-strained 2H clusters (~12%) distributed in the continuous 3C matrix.[21]

IV. DISCUSSION

To analyze the experimental findings, we will consider the growth models for both cases: 2H-AlN(0001)/3C-SiC/Si(111) and 3C-AlN(111)/3C-SiC/Si(111). In the simplest case, the growth mode is determined by the balance between the formation energies of the film surface σ_{film}, the template surface σ_{sub}, and the interfacial energy E_{int}. The formation energy of the 2D film E_{film} may be written as $E_{film}=\sigma_{film}-\sigma_{sub}+E_{int}$. A positive value for E_{film} implies that the island formation is favorable while a negative value implies that the 2D growth is stable. One can write the conditions for the 2D growth of a strained thin film as

$$\sigma_{sub} > \sigma_{film} + E_{int} - \Delta\mu/2A_{(hkl)} + n_{lat}E_{str}, \quad (1)$$

where $n_{lat}=3$ for hexagonal cell, E_{str} is the macroscopic stress energy, and $A_{(hkl)}$ is an intersection of the elemental cell with the surface plane (hkl). The free-surface energy σ is proportional to the atom density in the lattice plane N_S:

Downloaded 13 Jun 2005 to 141.24.27.92. Redistribution subject to AIP license or copyright, see http://jap.aip.org/jap/copyright.jsp

$$\sigma_{\text{surf}} = N_S^{(111)} \Delta H_f^{\text{AlN}} / 4N_a, \tag{2}$$

where N_a is the Avogadro constant. The reported free-surface energies of the interfacing materials are very similar: $\sigma_{\text{SiC}(111)} \cong 1.76\ \text{J m}^{-2}$, $\sigma_{\text{AlN}(0001)} \cong \sigma_{\text{AlN}(111)} \cong 1.8\ \text{J m}^{-2}$ [$\sigma_{\text{Si}(111)} \cong 1.24\ \text{J m}^{-2}$].[22,23] Thus, the growth dynamic should be determined by the remaining terms in Eq. (1)—the interface and epilayer formation energies.

The two last terms in Eq. (1) represent the formation energy of the epilayer.[24] $\Delta\mu = \mu - \mu_{\text{bulk}} = k_B T \ln S$ is a difference in the chemical potentials of the bulk and gas phases of the specie representing the actual growth conditions being a function of the supersaturation S and temperature T. The chemical potentials of the species (Al and N) are linearly dependent on each other by $\mu_{\text{bulk}}^{\text{AlN}} = \mu_{\text{Al}} + \mu_{\text{N}}$ ($\mu_{\text{bulk}}^{\text{AlN}} \cong -16.40$ eV (Ref. 5)). Using the relation for the heat of formation of the AlN compound $-\Delta H_f^{\text{AlN}} = \Delta\mu_{\text{Al}} + \Delta\mu_{\text{N}}$ [$\Delta H_f^{\text{AlN}} \cong 3.28$ eV (Ref. 5)], the actual growth conditions can be described by the following relation:

$$\mu_{\text{Al}} = \mu_{\text{bulk}}^{\text{AlN}} - \mu_{\text{bulk}}^{\text{N}} + \Delta H_f^{\text{AlN}} + \Delta\mu_{\text{Al}}, \tag{3}$$

where $\Delta\mu_{\text{Al}} = -\Delta H_f^{\text{AlN}}$ and $\Delta\mu_{\text{Al}} = 0$ imply N-rich and Al-rich growth conditions, respectively. At low supersaturations, typical for the stochiometric growth, the term $\Delta\mu / 2A_{(hkl)} \cong 0.05\ \text{J m}^{-2}$ does not affect the overall energy balance. However, at higher supersaturations used for flatterning of the 3C-AlN surfaces, the energy balance is shifted towards a pure 2D growth. At the flat surface conditions, for the growing system is energetically favorable to introduce a stacking fault in the (111) plane initiating the growth of the thermodynamically stable 2H phase ($\Delta E_{\text{W-ZB}} \sim -18.41$ meV/at.).

Thus, two valuable terms in Eq. (1) remain to be analyzed—the macroscopic stress E_{str} and the interfacial energy E_{int}. A contribution of E_{int} to the total film energy is in a reverse proportion to the layer thickness. This dependence explains well the cubic→wurtzite AlN polytype transition in the epitaxial superlattices (TiN/AlN or VN/AlN) at the certain critical thickness of 2–6 nm.[17,18] In our case, this approach does not work due to the experimentally observed stable 3C-AlN epitaxy.

A contribution of the macroscopic stress energy E_{str} can be estimated on the basis of XRD and high-resolution transmission electron microscopy (HRTEM) analyses. The measured and reference lattice parameters of the grown epilayers derived from the reciprocal space mapping are summarized in Table I. In contrast to the growth on pure Si(111),[10] the epitaxy on carbonized silicon resulted in strong deviations from the ideal hexagonal lattice. Thus, 2H-AlN is grown strained with an a/c ratio shifted far away from the equilibrium value (tensile strain) forcing an extra stabilization of the 2H phase. In contrast, 3C-AlN grows practically relaxed with $(2/3c_{3c})/a_{3c}$ close to the ideal ratio (value smaller than the 2H reference), favoring the cubic polytype stabilization.

In Table II, the values of the calculated residual stress for three heteroepitaxial systems are listed. The atomic plane relation $m:n$ between the AlN, SiC, and Si fringes has been derived from the filtered HRTEM images [approximate matching of $m(hkl)_f$ atomic planes of the epilayer with $n(hkl)_s$ planes of the substrate, $(hkl)_f \| (hkl)_s$]. For nonpseudomorphic systems such as AlN/Si and SiC/Si, such $m:n$ lattice matching relaxes a main part of the biaxial strain directly at the interface allowing continuous 2D mode growth.[10] The exact matching is usually achieved by the elastic strain in the film.

TABLE I. Lattice constants of the grown 3C- and 2H-AlN epilayers. For 3C-AlN(111), the ordinary cubic coordinate (a_0) has been transformed to the hexagonal coordinates (a,c) for a direct comparison to the 2H phase.

	Lattice constant (Å)	Reference value (Å)
a_{Si}	⋯	3.84
$a_{\text{3C-SiC}}$	⋯	3.08
a_{2h}	3.138	3.11
c_{2h}	4.962	4.98
a_{3c}	3.101	3.10
$2c_{3c}/3$	5.062	5.05
c_{2h}/a_{2h}	1.578	1.601
$(2c_{3c}/3)/a_{3c}$	1.629	1.630

It is not surprising that the most stable 2H-AlN/Si(111) 5:4-matched system represents a minimum in the macroscopic stress energy resulting in the stable 2D growth. Considering 3C-AlN/SiC on Si(111) and 2H-AlN on 3C-SiC/Si(111), the magnitude of the biaxial stress is high in both cases, but the 2H phase has a certain advantage (−10.9 GPa vs −9.7 GPa). This advantage plus the thermodynamical stability results in the stable 2H-AlN epitaxy on the flat RTCVD-SiC surface. Such highly strained 2H films have been grown in the 2D mode, with partial accommodation of the residual strain by the $b = 1/3\langle 11\bar{2}0\rangle$ treading dislocations.

To explain the observed stabilization of the 3C phase on the UHVCVD templates one important feature characteristic for the 3C-AlN/3C-SiC/Si(111) interfaces has to be considered. In the case of the flat surface conditions (RTCVD carbonization), a replication of the 3C template crystal structure is the long-range-order interatomic interaction (polytype structures differ in the relative position of the third neighbors along the ⟨111⟩ chain). The long-range-order lattice replication process can be easily overcome by the short-range ordering process forced by the thermodynamical stability of the 2H-AlN phase. Furthermore, in-plane (111) cell is biaxially strained ($\varepsilon_{xx} \sim -0.019$) and c lattice constant is free to relax up to $c_{2h}/a_{2h} \sim 1.578$ forcing extra 2H stability.

The UHVCVD-carbonized samples have a quite differ-

TABLE II. Calculated stress in the AlN/SiC/Si heterosystems. ε_{xx}, the biaxial strain; σ_{xx}, the biaxial stress (GPa); ε_u, the uniaxial strain; and σ_u, the uniaxial stress (GPa).

	3C-AlN/3C-SiC on Si(111)	2H-AlN on Si(111)	2H-AlN on 3C-SiC/Si(111)
$m:n$	62:49	5:4	1:1
ε_{xx}	−0.021	−0.012	−0.019
σ_{xx} GPa	−10.9	−6.1	−9.7
ε_u	0.1448	0.0678	0.0678
σ_u GPa	−9.3	−4.2	−6.7

Downloaded 13 Jun 2005 to 141.24.27.92. Redistribution subject to AIP license or copyright, see http://jap.aip.org/jap/copyright.jsp

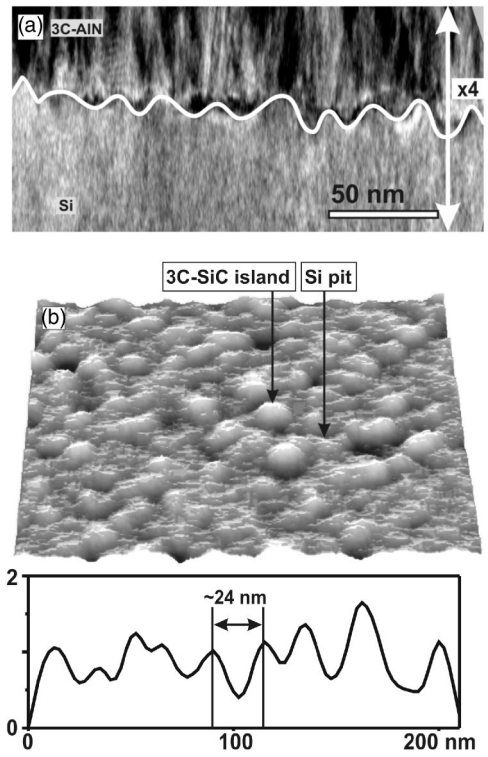

FIG. 5. Demonstration of the "waved" profile of UHVCVD-carbonized 3C-SiC/Si(111) template: (a) 110 bf-TEM image of the 3C-AlN/3C-SiC/Si(111)interface area. Phase contrast allows us to resolve 3C-SiC/Si(111) interface. (b) 200×200 nm^2 AFM image of 3C-SiC/Si(111) UHVCVD surface. Uniform distribution of the SiC islands determines a periodic modulation of the surface profile in arbitrary lateral direction.

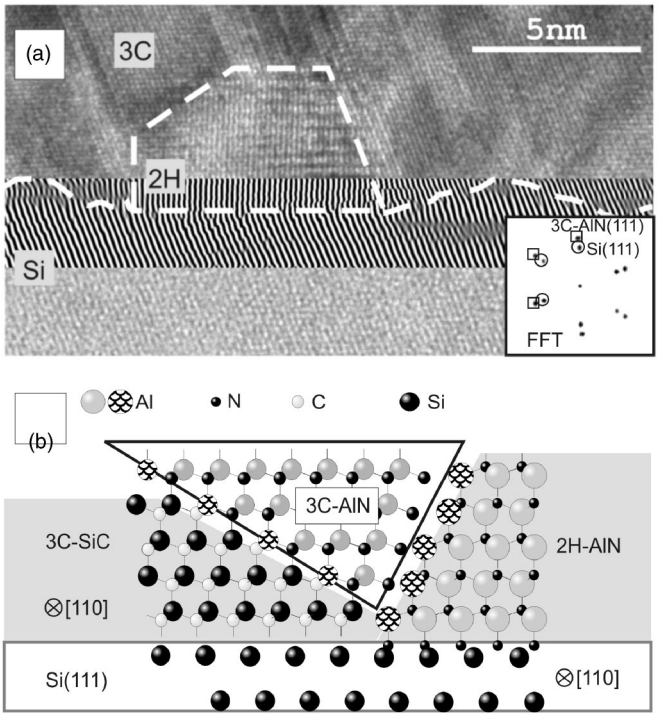

FIG. 6. (a) 110 bf-HRTEM-filtered images of the AlN/SiC/Si(111) interface demonstrates a 2H-AlN domain (marked by dashes) originating at the flat bottom of the Si pit formed during UHVCVD carbonization in the 3D mode [the image is fast Fourier transform (FFT) filtered at the interface area]. (b) Schematic view of the atomic arrangement at the interface.

ent surface morphology. Figure 5(a) demonstrates a 110 bf-TEM image of the 3C-AlN/3C-SiC/Si(111) interface area. The variations in the phase contrast in the 3C-SiC/Si(111) interface allows vs to resolve a periodically modulated surface profile with a period of ~24 nm. The observed features are a consequence of the UHVCVD carbonization mode. For the illustration of this phenomenon, a typical 200×200 nm^2 AFM scan image of 3C-SiC/Si(111) UHVCVD surface is shown in Fig. 5(b). One can see that uniform distribution of the SiC islands evocates a periodic modulation of the surface profile in arbitrary lateral direction. In general, the averaged period depends on the size and density of the SiC islands, which, in turn, are determined by the UHVCVD carbonization conditions. Under the typical experimental conditions, the island diameter and height range from 20 to 25 nm and from 0.5 to 2 nm, respectively. Taking into account the linear density of ~50 island/μm, the averaged profile period is ~24 nm.

The 3D morphology of the UHVCVD-SiC surface provides vicinal planes for the nucleation [for instance, $\{\bar{1}21\}$, see Figs. 5(a) and 5(b)] forcing a lateral replication of the template structure and therefore, the stable formation of 3C-AlN nuclei and their subsequent growth. In contrast, the lateral nucleation of the 2H domains leads to the short-range topological incompatibility and a huge uniaxial strain ($\varepsilon_u \sim 0.018$), which suppress 2H formation and favor the 3C-AlN polytype growth. An example in Fig. 6(a) illustrates this phenomenon. It is shown that the 2H-AlN domain originates from the small region of the AlN/Si interface (Si pit). The 5:4 match measured corresponds to the usual relationship at the 2H-AlN(0001)/Si(111) interface. In contrast, 3C-AlN nucleation starts only on the Δ-shaped, SiC-covered surface. The dominant 3C phase overgrows the hexagonal inclusion forming incoherent 3C-2H boundaries.

Moreover, taking into account the homogeneous distribution and certain uniformity in the size and shape of the SiC islands resulting in periodical distortions of the interface profile, we can introduce a term ΔE_M in the Eq. (1):

$$\sigma_{\text{sub}} > (\sigma_{\text{film}} - \Delta E_M) + E_{\text{int}} - \Delta\mu/2A_{(hkl)} + n_{\text{lat}}E_{\text{str}}, \qquad (4)$$

where

$$\Delta E_M = (-\sigma_{xx}^2/2Y)(A\lambda/2) + 2A\sigma_{\text{sub}} \qquad (5)$$

states for the reduction in the total energy of the system due to the periodical undulations at the 3C-AlN/SiC interface.[24] $A \sim 0.5$–2.0 nm and $\lambda \sim 10$–25 nm are the amplitude and period of the interface modulations, respectively, and Y is the Young's modulus. Such reduction forces an additional stability of the 3C phase allowing formation of continuous 3C film at the initial stage of the growth. After the coalescence of the developed 3C-AlN nuclei, with rising thickness of the epilayers, the contribution of the ΔE_M and E_I terms in Eq. (4) is getting smaller. At this stage, the growth dynamic is determined mainly by the stress (E_{str}) and surface morphology (influenced by $\Delta\mu = k_B T \ln S$) of the growing layer as it was discussed above.

Downloaded 13 Jun 2005 to 141.24.27.92. Redistribution subject to AIP license or copyright, see http://jap.aip.org/jap/copyright.jsp

V. CONCLUSIONS

Summarizing, we conclude that the nucleation of 3C-AlN polytype can be stabilized on the 3C-SiC/Si(111) surface by the polytype replication due to (i) the lateral character of the AlN nucleation on nonbasal planes of the 3C-SiC/Si(111) template and (ii) the reduction in the total energy of the film provided by the periodical undulations at the film/template interface.

It was demonstrated that the 3D UHVCVD-SiC surface provides vicinal planes for the nucleation supporting the lateral growth of the metastable 3C-AlN phase, while lateral nucleation of the 2H phase is suppressed by the short-range topological incompatibility and the huge uniaxial strain. Reduction in the total energy forces an additional stability of the 3C phase allowing formation of continuous 3C film at the initial stage of the growth. The growth dynamic of the thicker films is determined mainly by the stress and surface morphology of the growing 3C-AlN layer. It was also experimentally confirmed that the high supersaturation conditions (Al-rich growth) induce the nucleation and growth of the stable 2H-AlN phase on the flat 3C-AlN surface proving a metastable character of the 3C polytype.

ACKNOWLEDGMENTS

The authors would like to thank Dr. Ana Cros for providing Raman spectra and Dr. Thomas Stauden for his technical assistance. This research was supported partly by the Thüringer MWFK (Project No. B609-02004). The authors also acknowledge an ONR NICOP (Grant No. 04PR02823-00).

[1] S. Nakamura *et al.*, Jpn. J. Appl. Phys., Part 1 **37**, L309 (1998).
[2] C. Miskys, J. Garrido, C. Nebel, M. Hermann, O. Ambacher, M. Eickhoff, and M. Stutzmann, Appl. Phys. Lett. **82**, 290 (2003).
[3] P. Lawaetz, Phys. Rev. B **5**, 4039 (1972).
[4] C. Yeh, Z. Lu, S. Froyen, and A. Zunger, Phys. Rev. B **46**, 10086 (1992).
[5] L. Ramos, J. Furthmüller, J. Leite, L. Scolfaro, and F. Bechstedt, Phys. Rev. B **68**, 085209 (2003).
[6] M. Miao and W. Lambrecht, Phys. Rev. B **68**, 155320 (2003).
[7] A. Rubio, J. Corkhill, M. Cohen, E. Shirley, and S. Louie, Phys. Rev. B **48**, 11810 (1993).
[8] V. Cimalla, V. Lebedev, U. Kaiser, R. Goldhahn, Ch. Foerster, J. Pezoldt, and O. Ambacher, Phys. Status Solidi C **2**, 2199 (2005).
[9] S. Pugh, D. Dugdale, S. Brand, and R. Abram, J. Appl. Phys. **86**, 3768 (1999).
[10] V. Lebedev and W. Richter, in *Vacuum Science and Technology: Nitrides as Seen by The Technology*, edited by T. Paskova and B. Monemar (Research Signpost, Kerala, 2002).
[11] N. Christensen and I. Gorczyca, Phys. Rev. B **47**, 4307 (1993).
[12] W. Lin, L. Meng, G. Chen, and H. Liu, Appl. Phys. Lett. **66**, 2066 (1995).
[13] H. Harima *et al.*, Appl. Phys. Lett. **74**, 191 (1999).
[14] D. Gerthsen, B. Neubauer, Ch. Dieker, R. Lantier, A. Rizzi, and H. Lüth, J. Cryst. Growth **200**, 353 (1999).
[15] T. Koizumi *et al.*, J. Cryst. Growth **201/202**, 341 (1999).
[16] E. Martinez-Guerrero, F. Chabuel, B. Daudin, J. Rouviere, and H. Mariette, Appl. Phys. Lett. **81**, 5117 (2002).
[17] G. Li, J. Lao, J. Tian, Z. Han, and M. Gu, J. Appl. Phys. **95**, 92 (2004).
[18] A. Madan, I. Kim, S. Cheng, P. Yashar, V. Dravid, and S. Barnett, Phys. Rev. Lett. **78**, 1743 (1997).
[19] V. Cimalla, W. Attenberger, J. Lindner, B. Strizker, and J. Pezoldt, Mater. Sci. Forum **338–342**, 285 (2000).
[20] Z. Ren, Y. Lu, H. Ni, T. Liew, B. Cheong, S. Chow, M. Ng, and J. Wang, J. Appl. Phys. **88**, 7346 (2000).
[21] A. Goni, H. Siegle, K. Syassen, C. Thompsen, and J. Wagner, Phys. Rev. B **64**, 35205 (2001).
[22] J. Gilman, J. Appl. Phys. **31**, 2208 (1960).
[23] C. Messmer and J. Billelo, J. Appl. Phys. **52**, 4623 (1981).
[24] J. Howe, *Interfaces in Materials* (Wiley, New York, 1997).

Downloaded 13 Jun 2005 to 141.24.27.92. Redistribution subject to AIP license or copyright, see http://jap.aip.org/jap/copyright.jsp